Hybrid Mesoporous Silica-Based Drug Carrier Nanostructures with Improved Degradability by Hydroxyapatite

Xiaohong Hao,[†,§] Xixue Hu,[‡,§] Cuimiao Zhang,[†] Shizhu Chen,[†] Zhenhua Li,[†] Xinjian Yang,[†] Huifang Liu,[†] Guang Jia,[*,†] Dandan Liu,[†] Kun Ge,[†] Xing-Jie Liang,[*,‡] and Jinchao Zhang[*,†]

[†]College of Chemistry & Environmental Science, Chemical Biology Key Laboratory of Hebei Province, Key Laboratory of Medicinal Chemistry and Molecular Diagnosis of the Ministry of Education, Hebei University, Baoding 071002, People's Republic of China and [‡]CAS Key Laboratory for Biological Effects of Nanomaterials and Nanosafety, National Center for Nanoscience and Technology, Beijing 100190, People's Republic of China. [§]X. Hao and X. Hu contributed equally to this work.

ABSTRACT Potential bioaccumulation is one of the biggest limitations for silica nanodrug delivery systems in cancer therapy. In this study, a mesoporous silica nanoparticles/hydroxyapatite (MSNs/HAP) hybrid drug carrier, which enhanced the biodegradability of silica, was developed by a one-step method. The morphology and structure of the nanoparticles were characterized by TEM, DLS, FT-IR, XRD, N_2 adsorption–desorption isotherms, and XPS, and the drug loading and release behaviors were tested. TEM and ICP-OES results indicate that the degradability of the nanoparticles has been significantly improved by Ca^{2+} escape from the skeleton in an acid environment. The MSNs/HAP sample exhibits a higher drug loading content of about 5 times that of MSNs. The biological experiment results show that the MSNs/HAP not only exhibits good biocompatibility and antitumor effect but also greatly reduces the side effects of free DOX. The as-synthesized hybrid nanoparticles may act as a promising drug delivery system due to their good biocompatibility, high drug loading efficiency, pH sensitivity, and excellent biodegradability.

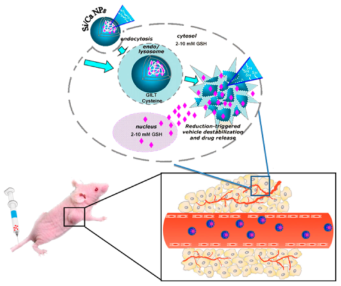

KEYWORDS: silica/hydroxyapatite hybrid nanoparticles · biodegradability · pH sensitivity · anticancer drug carrier

The delivery of drugs is an important area for human health. Drug delivery systems (DDSs) enable drugs and medical therapies to be much safer, more convenient, and more efficient.[1] A number of DDSs have emerged including polymeric nanoparticles[2] and nanocapsules,[3] liposomes,[4] micelles,[5] gold nanoparticles,[6] ceramic NPs, magnetic NPs, dendrimers, *etc.*[7] Several characteristics are desirable for materials used in drug delivery, such as a long shelf life, facile commercial synthetic scale up, and clearance from the body.[8] In recent years, inorganic nano/micromaterials have attracted much attention as drug carriers due to their excellent biocompatibility, bioactivity, low susceptibility to immune response, and resistance to lipases and bile salts.[9] Because silicon is a common trace element in humans and biocompatible with organisms, the design and synthesis of mesoporous silica nanoparticles, which exhibit large surface areas, well-defined surface properties, and high drug loading capacity, have become a hot research topic.[6,10–13]

A desirable design would involve carrier self-destruction, through which the carrier could be hierarchically degraded into harmless and clearable products.[14,15] It is well known that the degradation of pure silica is quite slow due to its stable network structure. As a result, the poor degradability of silica limits its biomedical applications due to the potential of inert nanoparticles bioaccumulating in the body.[16,17] Silica nanoparticles have been found to accumulate in the liver, bladder, kidneys, spleen, and lungs, which may cause severe problems and would do harm to living organs.[18–22] For instance, silica nanoparticles may induce severe liver damage in mice and inflammatory responses *in vitro*.[23,24] Therefore, the degradation of mesoporous silica nanoparticles (MSNs) is of great significance for their applications in biomedical fields. Yamashita *et al.* discovered that silica nanoparticles with a size of about 70 nm could be resorbed by placental trophoblasts, fetal liver, and fetal brain and restricted growth in pregnant mice, even causing complications at high concentrations.[25]

* Address correspondence to
guangjia2001@163.com,
liangxj@nanoctr.cn,
jczhang6970@163.com.

Received for review December 31, 2014
and accepted August 28, 2015.

10.1021/nn507485j

On the other hand, biodegradable drug carriers can facilitate the surgical removal of carriers and reduce the damage caused by carrier accumulation. Hence it is of great significance and highly desirable to fabricate degradable silica drug carriers. During the past decade, various methods have been proposed to improve the degradability of silica nanoparticles. For instance, Pohaku Mitchell *et al*. doped iron(III) into hollow silica nanoshells during sol−gel synthesis, and the as-obtained material can be degraded by removal of iron even after calcination; yet whether the nanoparticles can be used as a drug carrier with high loading efficiency and controllable release behavior or are toxic to cells and animals remains to be investigated.[26] Li *et al*. reported that the addition of calcium ions into silica spheres improved the degradation and bioactivity of silica spheres, but the basal morphology of the nanoparticles was not significantly changed even after the degradation for 3 days.[27] Therefore, it still remains a challenge to develop silica-based drug delivery systems with low toxicity, good biocompatibility, and excellent degradability.

Insufficient intracellular drug release from nanoparticles always limits the amount of anticancer drugs that actually reach cancer cells, which not only hampers the efficacy of cancer chemotherapy but also induces toxic side effects in the body. To conquer the challenges, stimuli-responsive valves or gatekeepers for the controlled release of drug molecules from mesoporous silica nanoparticles have been developed.[28,29] To date, various physical/chemical stimuli have been used as triggers for uncapping the pore blockers and releasing encapsulated guest molecules and thus achieved highly efficient delivery of drug into tumors with minimal patient side effects.[30−32]

In this paper, a novel degradable and pH-responsive mesoporous silica nanoparticles/hydroxyapatite (MSNs/HAP) hybrid drug carrier has been fabricated by homogeneously incorporating calcium salt into silica nanoparticles. The incorporation of HAP not only enhances the degradability but also improves the drug loading amount, drug release efficiency, and pH sensitivity of the particles. The cytotoxicity, drug release behavior, and antitumor effect of the hybrid materials were also investigated *in vitro* and *in vivo* and indicate that the as-synthesized MSNs/HAP hybrid material can be used as an attractive and promising drug delivery system for therapeutic applications.

RESULTS AND DISCUSSION

Synthesis and Characterizations of MSNs and MSNs/HAP. In order to achieve an optimal controllable delivery system that can exhibit less cytotoxicity, higher loading capacity, better pH responsiveness, and biodegradable properties, the MSNs/HAP hybrid material was synthesized. Figure S1 in the Supporting Information shows the thermogravimetric (TG) curves of MSNs and MSNs/HAP samples, which indicates that the decomposition of cetyltrimethylammonium bromide (CTAB) is virtually complete at ∼500 °C, yet most was removed at 300 °C. To ensure the complete removal of the surfactant while the samples are well maintained, we choose the sintering condition of 400 °C for 2 h. The as-obtained nanoparticles were also characterized by transmission electron microscopy (TEM), dynamic light scattering (DLS), Fourier transform infrared spectroscopy (FT-IR), and X-ray diffraction spectra (XRD) to determine the structure, morphology, and particle size, as shown in Figure 1. One can see that the MSNs exhibit ordered mesostructures and spherical morphology (Figure 1a,b), while the MSNs/HAP is composed of novel hybrid spherical nanoparticles with unique skeletal structure of continuous walls and obvious holes (Figure 1c,d). The small-angle XRD patterns (Figure S2 in the Supporting Information) of the MSMs and MSNs/HAP ensure the existence of a high degree of well-ordered mesoporous structure,[33,34] which is in agreement with the TEM analysis. From the DLS analysis, it can be seen that the MSNs and MSNs/HAP samples are uniform in a narrow size distribution with diameters of 80−90 nm (Figure 1e,f), which agrees well with the TEM observations.

Figure 1g and h present the XRD patterns of MSNs and MSNs/HAP. The amorphous hump of MSNs in the region between about 15° and 40° is bated by some sharp peaks after incorporation of calcium salt during the synthesis process. The generated sharp peaks can be well assigned to the hexagonal hydroxyapatite (JCPDS 09-0432), which indicates that the hydroxyapatite has been successfully embedded into the skeleton of MSNs. Figure 1i and j show the FT-IR spectra of MSNs and MSNs/HAP. For MSNs (Figure 1i), the bands centered at 2600−3700 and 1636 cm^{-1} are respectively due to O−H stretching and adsorbed water. The strong absorption peaks in the framework region at about 1088, 805, and 466 cm^{-1} are generally attributed to stretching vibrations of Si−O−Si, bending vibrations of O−Si−O, and rocking vibrations of Si−O−Si, respectively. The FT-IR spectrum of MSNs/HAP is similar to that of the MSN sample (Figure 1j). The characteristic asymmetric stretching vibrations of $\mathrm{PO_4}^{3-}$ groups overlap with the stretching vibration band of Si−O−Si at about 1084 cm^{-1}.[35,36] Moreover, it is notable that the peaks at 569, 607, and 670 cm^{-1} can be attributed to a Si−O−Ca asymmetric bending mode.[37] Furthermore, the existence of Si−O−Ca was also demonstrated by the analysis of X-ray photoelectron spectroscopy (XPS) spectra, as shown in Figure S3 in the Supporting Information. The result indicates that the addition of calcium salt into the reaction system causes the introduction of Ca^{2+} ions into the silica network and damages some silicon oxygen bonds with the production of Si−O−Ca−O−Si-type groups.

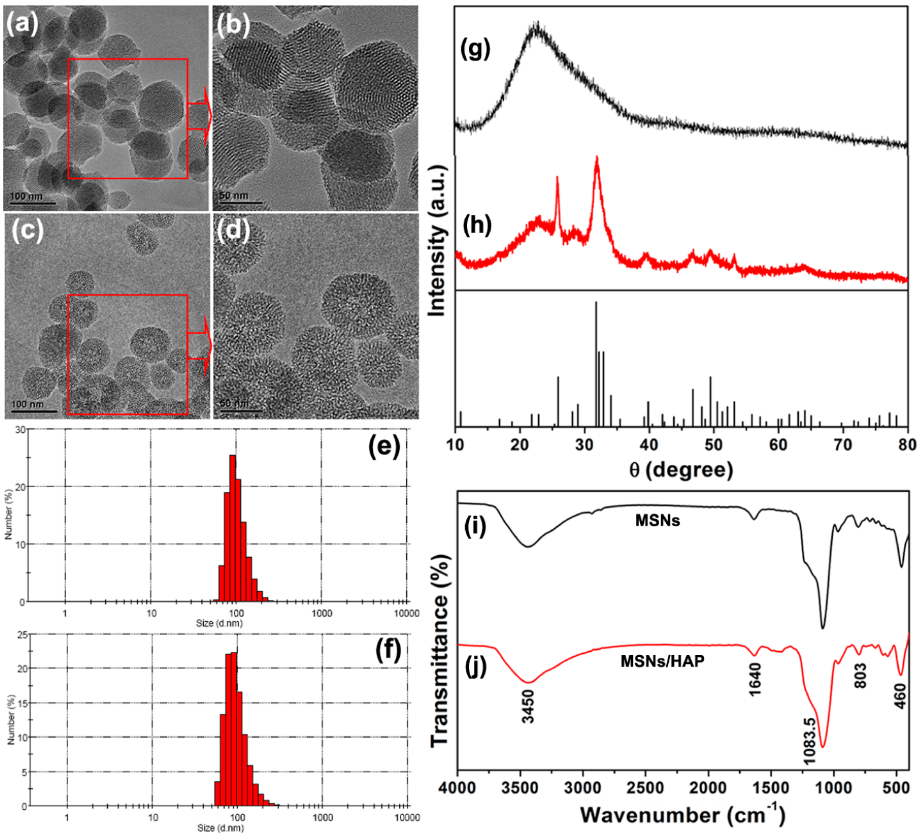

Figure 1. Physicochemical characterizations of MSNs and MSNs/HAP samples: TEM images of (a, b) MSNs and (c, d) MSNs/HAP; size distribution of (e) MSNs and (f) MSNs/HAP; XRD patterns of (g) MSNs and (h) MSNs/HAP; FT-IR spectra of (i) MSNs and (j) MSNs/HAP.

To further study the structure of the MSNs/HAP comprehensively, the element signals in the particle surface and ensemble distribution of silicon, phosphorus, calcium, and oxygen were investigated by Tecnai G2 F20 U-TWIN and XPS measurement. Figure 2a and b confirm that MSNs/HAP contained silicon (Si), oxygen (O), calcium (Ca), and phosphorus (P) elements, and the four elements are uniformly distributed in the nanoparticles. The texture parameters of the samples were tested by the low-temperature nitrogen adsorption–desorption method. The specific surface area and the pore size distribution are determined by the BET method and BJH model, respectively. As shown in Table 1, the MSN sample exhibits a high specific surface area (~1500 $m^2 \cdot g^{-1}$) and a mesoporous structure of ~2 nm (Figure 2c). However, the BET surface area of MSNs/HAP decreases to 543 $m^2 \cdot g^{-1}$, and the MSNs/HAP sample has a complicated porous structure changing from about 2 nm to 16 nm (Figure 2d). The large size of the pores makes it suitable for high drug loading efficiency, which is important for drug carriers.

Nanoparticle Degradation. MSNs have been considered to be a promising drug carrier because of their mesoporous structure and good biocompatibility. However, the poor biodegradability of MSNs greatly limits their *in vivo* biomedical applications. In various previous studies, it is reported that the MSNs can accumulate in the liver, bladder, spleen, kidneys, and lungs,[18−21,38] which may induce damage of the organs. Therefore, great efforts have been devoted to improve the biodegradability of MSNs. Pohaku Mitchell reported an interesting route to facilitate the biodegradability of silica nanoparticles by doping ferric irons into the silica structure.[25] The silica can degrade on removal of iron(III) within several days at 80 °C. The degradation process takes a long time and a relatively high temperature (much higher than physiological temperature), which may seriously limit the biological applications of the iron(III)-doped silica materials. Therefore, it is highly desirable to design biodegradable MSNs, which can be degraded at physiological temperature for a relatively short period of time. In the present study, the biodegradability of the as-synthesized MSNs and MSNs/HAP materials was investigated at different pH values. *In vitro* degradation is determined by suspending the material in acidic buffer solution, which to some extent imitates the acidic environment at the tumor area. The nanoparticles collapsed and dispersed into smaller or soluble fragments due to the defects in the structure caused by the removal of Ca^{2+} ions from the site. The morphology of nanoparticles after degradation was observed by TEM, and the release of Ca^{2+} ions was monitored as the degradation time increased, as shown in Figure 3. The observation

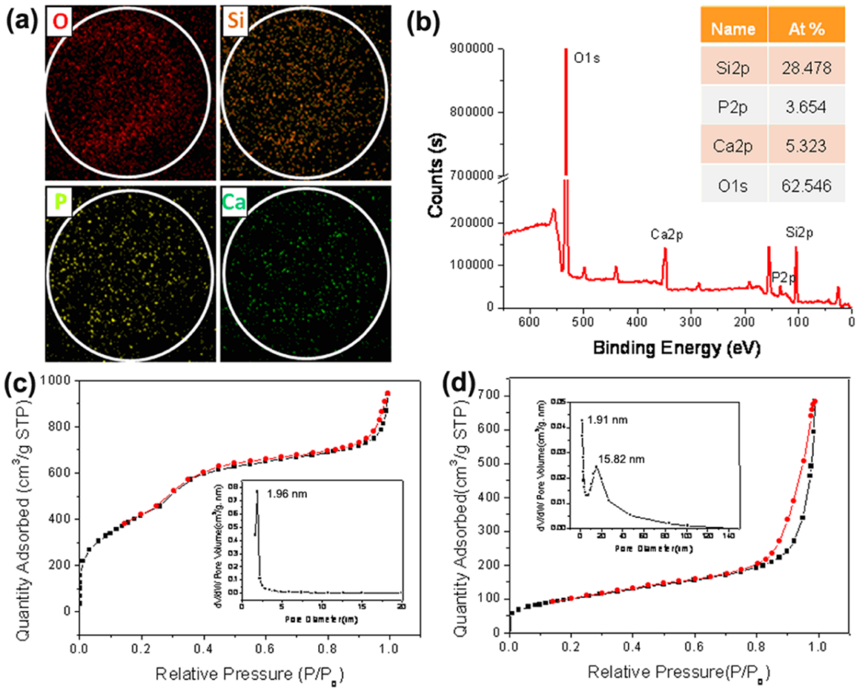

Figure 2. (a) Element distribution, (b) XPS analysis of MSNs/HAP and N_2 adsorption–desorption isotherms, and pore size distributions (the insets) of (c) MSNs and (d) MSNs/HAP.

TABLE 1. BET Surface Area, Pore Diameter, and Drug Loading Efficiency of MSNs and MSNs/HAP Samples

nanoparticles	BET surface area (m^2/g)	pore diameter (nm)	drug loading efficiency (%)
MSNs	1546.13	1.96	13.98
MSNs/HAP	542.66	1.94 and 15.82	33.06

of TEM reveals that the MSNs/HAP nanoparticles become scattered debris after 4 h at pH 5 in acid buffer solution, as shown in Figure 3b,c. When the time is extended to 12 h, the nanoparticles are broken into many fragments with a size of about 20 nm (Figure 3d, e). The significant difference of the Ca^{2+} ions' release in pH = 7.4 and pH = 5.0 exhibits obvious pH sensitivity of the MSNs/HAP. The Ca^{2+} ions in MSNs/HAP are almost completely removed in acid buffer solution (pH 5) after 8 h (Figure 3f). However, the Ca^{2+} ions cannot be released from MSNs, and the morphology of MSNs exhibits no change after treatment at pH 5 for 12 h (Figure S4 in the Supporting Information). The improved degradability of the nanoparticles might be attributed to the degradability of hydroxyapatite embedded in the particles and the removal of Ca^{2+} ions from the structure of Si–O–Ca. As we know, good degradability is very important for drug carriers because the biodegradable drug carriers can reduce the damage caused by carrier accumulation. In this case, the HAP component in MSNs/HAP can be easily dissolved in acid buffer solution, which can be confirmed by the TEM and the release of Ca^{2+} ions. Then, the complete removal of HAP induces the collapse of the silica network, resulting in the degradation of MSNs/HAP nanoparticles. As the lysosomal pH value differs among different cancer cells, the degradation properties of the MSNs/HAP sample were also investigated in acid buffer solution at different pH values (6.0 and 4.5) for 12 h. It can be found from the TEM images that the MSNs/HAP nanospheres are broken and degraded into smaller aggregated nanoparticles when treated at pH 6.0. On further decreasing the pH value to 4.5, the MSNs/HAP sample is completely destroyed and almost degraded into tiny nanofragments (Figure S5 in the Supporting Information). The results indicate that the as-synthesized MSNs/HAP sample can be easily degraded in acidic buffer solution at physiological temperature and may be potentially applied as pH-responsive drug carriers in the biomedical field.

In vivo, extensive studies revealed that the injected MSNs accumulated mainly in the tumor and mononuclear phagocyte system (MPS)-related organs such as the liver and spleen, and the MSNs accumulated in the organs are noticeably cleared from the body within a period of 1 week and completely cleared in 4 weeks.[15,39−41] In this study, the *in vivo* biodistribution and degradation properties of MSNs and MSNs/HAP particles were also investigated in an animal setting. We tested the accumulated concentration of Si element by ICP-OES at two time points (24 and 48 h) postinjection of MSNs and MSNs/HAP to explore how the nanoparticles behave in animals. It can be found that both the injected MSNs and MSNs/HAP

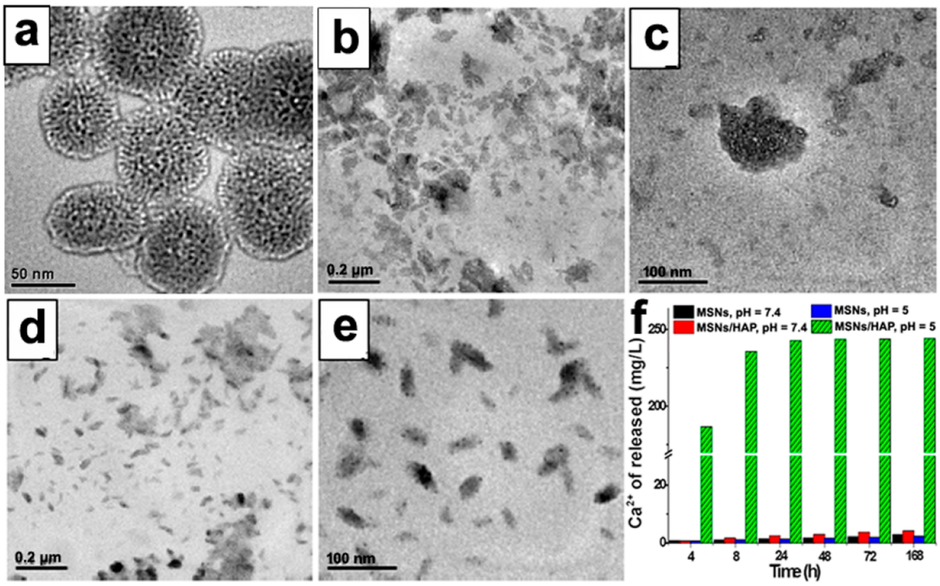

Figure 3. TEM images of the MSNs/HAP sample after degradation in acid buffer solution (pH 5.0) for (a) 0 h, (b, c) 4 h, (d, e) 12 h; (f) the release of Ca^{2+} at pH = 7.4 and 5.0.

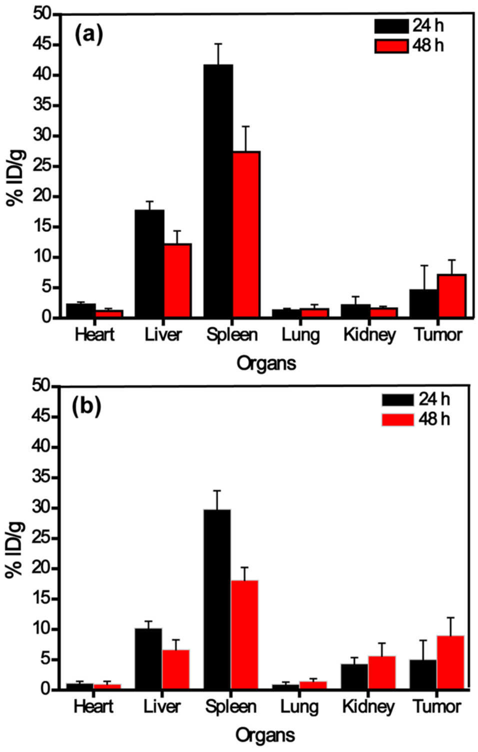

Figure 4. ICP-OES analysis of Si amounts in the organs of mice collected at 24 and 48 h after injection of (a) MSNs and MSNs/HAP.

accumulated mainly in the mononuclear phagocytic system-related organs such as the liver and spleen (Figure 4), which agrees well with the previous reports.[15,39] However, an increase of accumulated concentration of Si element in the kidney was observed in the MSNs/HAP group in comparison with the MSN group. It has been indicated that the inorganic nanoparticles with diameters of <5.5 nm were easy to excrete *via* renal clearance.[14] After the degradation of MSNs/HAP, more small fragments accumulated in the kidney, then were excreted *via* renal clearance. Furthermore, we qualitatively tested the excreted small fragments in urine by fluorescence labeling of MSNs/HAP (Figure S6 in the Supporting Information). Enhanced fluorescence was observed in the MSNs/HAP group, which was attributed to the generation of small fluorescent fragments from MSNs/HAP.

Doxorubicin (DOX) Loading and Release Study. Due to the uniform spherical morphology, mesoporous structure, high surface area, and excellent biodegradability, the as-obtained MSNs/HAP hybrid material may be potentially applied as a promising drug carrier in the biomedical field. The drug loading efficiency of the potential drug carriers is shown in Table 1. It can be seen that the MSN sample exhibits low DOX adsorption, while more DOX, approximately 2.4 times, is loaded into the MSNs/HAP sample. The mass percentage and absolute mass of cumulative released DOX from the nanocarriers are shown in Figure 5a,b. An initial burst in the first 12 h appears, and then the drug released from MSNs stays almost constant during the next 6 days. However, for the MSNs/HAP, different DOX release kinetics can be observed, showing a two-step release pattern with an initial burst release and a relatively slow sustained release over 6 days. After 7 days, the cumulative release rate reached 31.69% and 58.06% for MSNs and MSNs/HAP, respectively. Compared to their release rate of 38.79% and 81.48% at pH 5.0, pH-sensitive release capabilities of drug for MSNs/HAP exhibit a remarkable increase. The accelerated release of loaded drug is attributed to the degradation of MSNs/HAP into smaller size nanoparticles. We calculated the released DOX amount per 10 mg carrier,

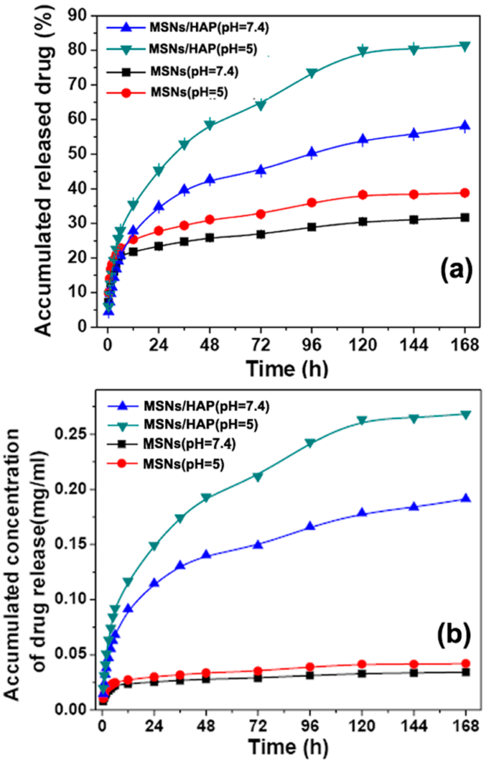

Figure 5. (a) Mass percentage and (b) absolute mass of cumulative released DOX from DOX@MSNs and DOX@MSNs/HAP in buffer solutions (pH = 7.4 and 5.0) at 37 °C.

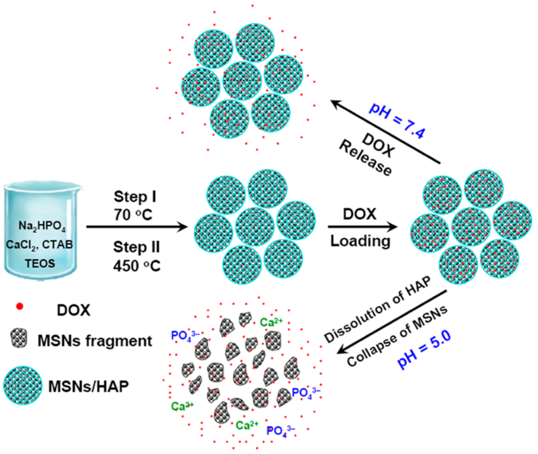

Scheme 1. Schematic illustration of the synthesis, drug loading and controlled release, and degradation process of MSNs/HAP composites.

as shown in Figure 5b. A tremendous difference of drug-loaded amount between the MSNs and the MSNs/HAP was observed. The final released DOX from MSNs/HAP is about 8 times that of MSNs. It could be seen that the MSNs/HAP exhibits an excellent pH-responsive release property, which can be assigned to the breakdown of the nanoparticles in an acid environment. A schematic representation of the rational design employed to obtain MSNs/HAP composites, subsequent degradation, and the drug storage/release process is shown in Scheme 1.

Biocompatibility and Anticancer Effect of the Nanoparticles. To evaluate the potential of MSNs/HAP as an effective drug carrier for cancer therapy, the *in vitro* cytotoxicity of MSNs, MSNs/HAP, DOX@MSNs, and DOX@MSNs/HAP was investigated. The impact of nanoparticles on red blood cells (RBCs) was evaluated by a hemolysis assay.[42−44] The quantitation of hemoglobin in the supernatant of a nanoparticle RBC mixture was performed by recording the absorbance. As shown in Figure S7 in the Supporting Information, the extent of hemolysis is dose-dependent for MSNs; especially the concentrations of 400 and 800 μg/mL result in severe hemolysis. In contrast, the MSNs/HAP group exhibits almost no hemolysis at all the tested concentrations. Obviously, the MSNs/HAP sample has better hemocompatibility than MSNs. Moreover, *in vitro* cytotoxicity of the nanoparticles on MCF-7 cells was also investigated by the MTT assay. MCF-7 cells were incubated with MSNs, MSNs/HAP, DOX@MSNs, and DOX@MSNs/HAP, and the concentration of DOX was used as an equivalent concentration in all the biology experiments. It could be seen from Figure 6a that MSNs/HAP has better biocompatibility compared with MSNs. Moreover, DOX@MSNs/HAP exhibits a good anticancer effect on MCF-7s cells, even comparable to that of free DOX (Figure 6b).

To verify pH responsive release behavior of DOX@MSNs/HAP in cells, the intracellular DOX distribution was analyzed by using DOX autofluorescence after incubation for 4 h. Lysotracker Green, a specific probe for acidic compartments, was used to confirm the lysosome colocation of DOX@MSNs/HAP. In the group of cells treated with DOX@MSNs and DOX@MSNs/HAP, most DOX gathered in the lysosomes, of which the fluorescence overlapped with that of the Lysotracker, and some DOX dispersed in the cytoplasm, surrounding the lysosomes, as shown in Figure 6c.

The effect of DOX delivery to the tumor by nanoparticles was further determined *in vivo*. To this end, we implanted first human breast cancer cells MCF-7 in the left armpit skin of nude mice. After tumor establishment, the mice were then given continuous therapy by tail vein injection twice every week with phosphate-buffered saline (PBS, control group), free DOX, DOX@MSNs, or DOX@MSNs/HAP at equivalent DOX doses of 0.3 mg/kg. To assess the antitumor effect and the toxic effects in mice, the change of tumor volume and relative body weight are recorded in Figure 7. The results indicate that the sustained administration with different DOX formulations is capable of slowing tumor growth compared to control treated mice, and the treatment with DOX@MSNs and DOX@MSNs/HAP has more effect on suppressing the tumor development than free DOX (Figure 7a,b). Notably, the inhibition effect of DOX@MSNs/HAP (54.8%) on the tumor is the best for all the agents, which is superior to DOX@MSNs (38.8%). On the other hand, no significant change was observed after treatment with the nanoparticles

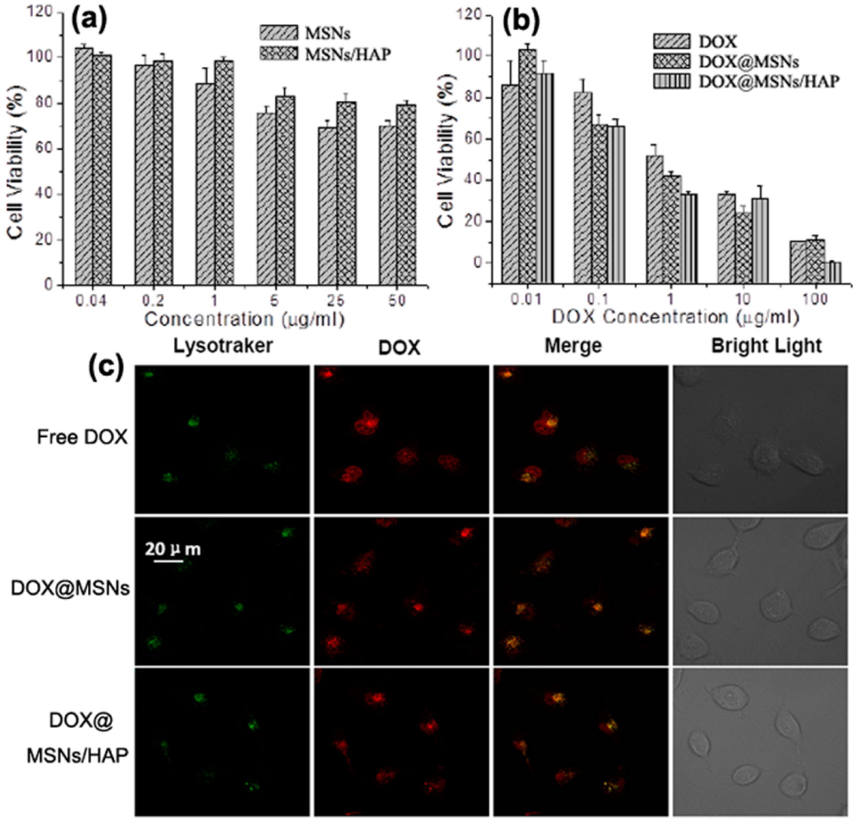

Figure 6. (a, b) Biocompatibility and (c) cellular uptake and intracellular drug release of the samples.

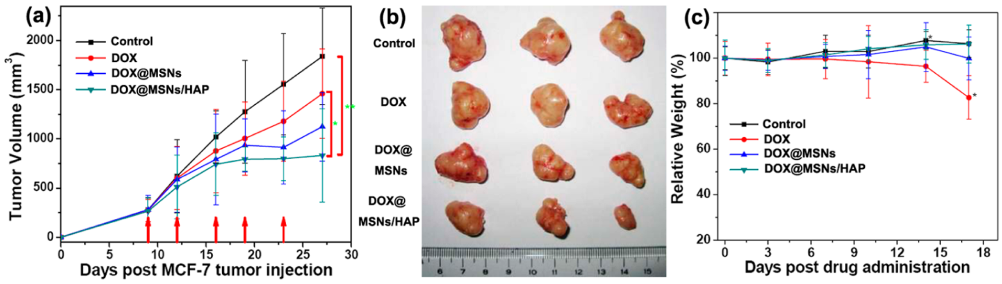

Figure 7. (a, b) Tumor growth inhibition effect and (c) body weight change upon treatment with DOX, DOX@MSNs, and DOX@MSNs/HAP.

of DOX@MSNs and DOX@MSNs/HAP in terms of mouse body weights (Figure 7c). However, the group treated with free DOX showed a fast loss of body weight, which is mainly caused by the side effects of the drug.

Biochemical Assay of Serum and Histological Analysis. Blood biochemical tests can monitor the response to exogenous toxic exposure and are widely used in disease diagnoses of the liver, kidney, *etc.*[45] The changes in biochemical parameters of the DOX, DOX@MSNs, and DOX@MSNs/HAP groups are presented in Table 2. The blood biochemical tests of total bilirubin levels (TBIL), alanine aminotransferase (ALT), aspartate aminotransferase (AST), and AST/ALT are widely utilized to evaluate liver function. When the liver is in dysfunction, the levels of the aforementioned enzymes rise. For the DOX group, the AST level ($p < 0.05$) and AST/ALT level ($p < 0.05$) increase significantly compared with the control group. The elevated levels indicate that the hepatic dysfunction might be induced by DOX. However, there is no significant change of above parameters in the DOX@MSNs and DOX@MSNs/HAP groups ($p > 0.05$). Correspondingly, the blood uric acid (UA), creatinine (Cr), blood urea nitrogen (BUN), and total protein (T-prot) are good indicators of renal function. If renal function is deteriorated, the UA, BUN, and T-prot levels rise. For the DOX group, the BUN/Cr increases significantly in contrast with the control group ($p < 0.01$). However, the levels of these parameters in the DOX@MSNs and DOX@MSNs/HAP groups are similar to those of the control group ($p > 0.05$). These results show that the treatments of DOX@MSNs and DOX@MSNs/HAP have

TABLE 2. Changes of Biochemical Parameters in the Serum of Mice ($n = 3$, mean ± SD)

groups	TBIL (umol/L)	ALT (U/L)	AST (U/L)	AST/ALT	UA (umol/L)	BUN (mmol/L)	Cr (umol/L)	BUN/Cr(10^3)	T-prot (g/L)
control	0.26 ± 0.15	40.76 ± 5.98	225.34 ± 25.42	5.42 ± 0.32	381.46 ± 39.64	8.38 ± 0.53	17.66 ± 5.57	0.52 ± 0.19	55.86 ± 3.52
DOX	0.28 ± 0.05	35.18 ± 4.09[a]	296.87 ± 43.44[a]	8.41 ± 0.80[b]	339.10 ± 67.61	7.94 ± 0.67	8.40 ± 0.81[a]	0.95 ± 0.13[b]	54.93 ± 3.89
DOX@MSN	0.18 ± 0.10	43.08 ± 5.59	238.48 ± 32.42	5.54 ± 0.36	335.35 ± 44.57	7.44 ± 1.14	15.18 ± 4.05	0.54 ± 0.25	54.23 ± 3.11
DOX@MSNs/HAP	0.35 ± 0.21	43.40 ± 6.93	232.40 ± 22.20	5.47 ± 1.38	316.20 ± 51.76	6.49 ± 0.33	9.70 ± 5.37	0.80 ± 0.48	55.10 ± 57.67

[a] $p < 0.05$ *vs* the control group. [b] $p < 0.01$ *vs* the control group.

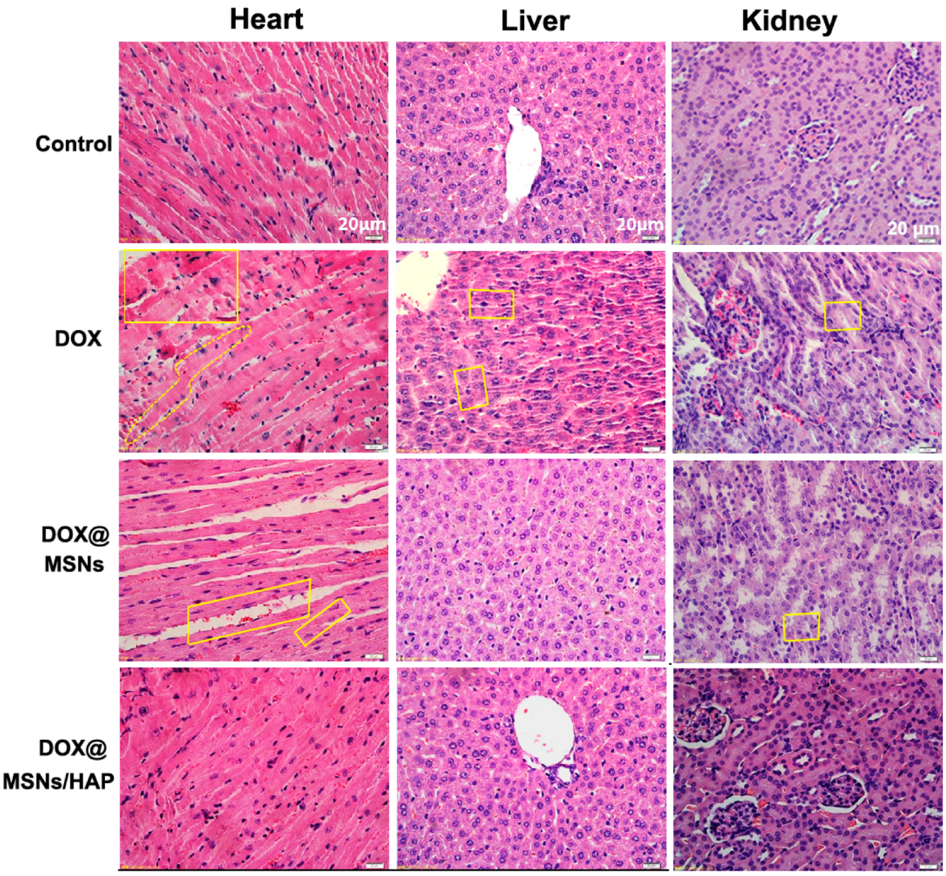

Figure 8. Histological evaluation from the major damaged organs of mice treated with saline (control group), DOX, DOX@MSNs, and DOX@MSNs/HAP.

no negative effects on the mouse liver and kidney, but the injection of free DOX might cause liver and kidney injury.

Figure 8 shows the histopathological findings of the heart, liver, and kidney. For heart tissue, the DOX group resulted in more severe injury, such as ischemic lesions, necrosis, or dissolution of myocardial cells, while the DOX@MSNs group shows slight myocardial interstitial edema and congestion of the myocardial matrix. In contrast, the DOX@MSNs/HAP group exhibits no significant lesions in the heart. Since the release of DOX from the DOX-loaded MSNs/HAP is more controllable than DOX-loaded MSNs, there is no acute release to cause clear myocardial interstitial edema. However, the release of DOX from the DOX-loaded MSNs is uncontrollable, which caused the acute release of DOX in the heart, inducing myocardial interstitial edema. For the liver, necrosis of hepatocytes and bile duct injury are observed in the DOX group, and the DOX@MSNs and the DOX@MSNs/HAP groups reveal no significant lesions. For the effect on the kidney, necrosis of renal tubular epithelial cells in the DOX group can be observed. The clinical renal lesions of the DOX@MSNs group exhibit mild edema, and there are no significant lesions in the DOX@MSNs/HAP group. It can be seen from the above results that the DOX@MSNs/HAP group shows few histopathological abnormalities, lesions, and degenerations of the major organs (including heart, liver, and kidney), which indicates little cell and tissue damage is induced by DOX@MSNs/HAP. In contrast, there are different degrees of damage for the heart, liver, and kidney of the mice treated with free DOX and DOX@MSNs. The results demonstrate that the MSNs/HAP drug delivery system has advantages of improved antitumor efficacy and reduced side effects and, thus, may be used as an attractive and promising drug carrier for therapeutic applications.

CONCLUSIONS

In conclusion, we successfully demonstrate a degradable drug carrier fabricated by homogeneously incorporating hydroxyapatite into a silica lattice, which not only has improved drug loading amount and drug release efficiency but also exhibits pH-responsive drug release from the hybrid nanoparticles. In particular, the breakdown of MSNs/HAP nanospheres could improve the penetration ability and release efficiency of the loaded drug into tumor tissues. The antitumor result of DOX@MSNs and DOX@MSNs/HAP *in vitro* and *in vivo* indicates that DOX@MSNs/HAP might be more effective in cancer treatment. The biochemical and histopathological tests also reveal that the alternative of the MSNs/HAP drug carrier may be safer and has attractive *in vivo* application prospects.

EXPERIMENTAL SECTION

Materials. Cetyltrimethylammonium bromide (CTAB), tetraethyoxysilane (TEOS), and 3-(4,5)-dimethylthiahiazo(-2-yl)-3,5-diphenyltetrazolium bromide (MTT) were purchased from Sigma-Aldrich (St. Louis, MO, USA). Calcium chloride anhydrous ($CaCl_2$) and disodium hydrogen phosphate dodecahydrate ($Na_2HPO_4 \cdot 12H_2O$) were obtained from Shanghai Chemical Reagents Company (Shanghai, China). Five- to six-week-old athymic BALB/c nude female mice of 16 ± 1 g weight were purchased from Beijing Vitalriver Experimental Animal Technology Co. Ltd. TBIL, ALT, and AST were purchased from Beijing Capital Medical University Clinical Science Center. UA, BUN, and Cr assay kits were purchased from Randox Laboratories Ltd. UK.

Synthesis of MSNs and Degradable MSNs/HAP. MSNs were synthesized according to our previous literature report.[46] In a typical synthesis, 7 mL of a 0.2 M NaOH aqueous solution was added into 96 mL of water under stirring, followed by the addition of 200 mg of CTAB. The pH value of the solution was 11. The solution was heated to 70 °C with vigorous stirring and kept for 30 min. Then 1 mL of TEOS was added dropwise under vigorous stirring. The gradual change of solution from clear to opaque indicated a hydrolysis process. The reaction was kept at 70 °C for 4 h. The product was collected by centrifugation and washed twice with H_2O and methanol, respectively. In order to remove the CTAB, the collected particles were suspended in the mixing solution with 50 mL of methanol and 2.0 mL of 12 M hydrochloride acid. The solution was refluxed for 10 h, and the product was collected by centrifugation and washed with methanol (denoted as MSNs).

For the synthesis of mesoporous silica nanoparticles/hydroxyapatite hybrid material (denoted as MSNs/HAP), $CaCl_2$ and $Na_2HPO_4 \cdot 12H_2O$ were used as a source of Ca^{2+} and PO_4^{3-} ions, respectively. In a typical procedure, 7 mL of a 0.2 M NaOH aqueous solution was added into 96 mL of water under stirring, followed by the addition of 200 mg of CTAB (pH 11). Then, 0.3214 g of $Na_2HPO_4 \cdot 12H_2O$ was introduced to the above solution. After the mixture solution was stirred for 30 min at 70 °C, 0.9 mL of TEOS was added dropwise under vigorous stirring. Subsequently, 2 mL of solution containing 0.1494 g of $CaCl_2$ was added to the solution immediately, in which the molar ratio of Ca to Si was 1:3. Then the solution turned turbid, and the reaction was kept at 70 °C for 4 h. The product was collected by centrifugation and washed twice with H_2O and methanol, respectively. Finally, the freeze-dried sample was calcined at 400 °C for 2 h to remove the CTAB and obtain the final MSNs/HAP sample.

Characterizations. The morphology of the samples was observed using a Tecnai G2 20 S-TWIN TEM (Philips, FEI Company) operating at a 200 kV acceleration voltage. Thermostability of the samples was tested under a nitrogen atmosphere by a thermogravimetric analyzer (TGA). The size distribution of the samples was obtained by DLS (ZetaSizer Nano ZS, Malvern Instruments Ltd., Worcestershire, UK). FT-IR spectra were recorded with a Spectrum One FT-IR spectrometer (PerkinElmer Instruments Co. Ltd., USA). The phase structure was characterized by XRD spectra (Bruker D8 Focus, Germany). N_2 adsorption–desorption isotherms were carried out on a Micromeritics ASAP2020 (M+C) analyzer (Micromeritics Instrument Corporation, USA) at 77.3 K under continuous adsorption conditions. Element distribution and surface element analysis were determined by using a Tecnai G2 F20 U-TWIN (FEI, USA) and an XPS (ESCALAB250Xi), respectively.

***In Vitro* Nanoparticle Degradation Process.** *In vitro* degradation behaviors of MSNs and MSNs/HAP were studied by immersing corresponding powders in different buffer solutions (pH = 7.4, 6.0, 5.0, and 4.5) at the concentration of 2 mg/mL at 37 °C. The change of morphology was observed by TEM. The released calcium was determined using the supernatant by centrifugation at certain time points by an Optima 5300DV inductively coupled plasma-optical emission spectrometer (ICP-OES, PerkinElmer, USA).

Animals and Treatment. The athymic BALB/c nude female mice were maintained under specific pathogen-free conditions. Sterilized pellet diet for mice and distilled water were available *ad libitum*. Mice were acclimated to the environment for 1 week before treatment, and the animal experiment was performed with the local approved protocols of the Administration Office Committee of Laboratory Animals.

Urinary Excretion and *in Vivo* Biodistribution, Degradation. For the urinary excretion investigation, nude mice were randomly divided into three groups ($n = 5$) and injected with fluorescein isothiocyanate-labeled MSNs/HAP and MSNs (20 mg/kg) or saline (control) through the tail vein. Special single-mouse metabolic cages were used. The urine was collected into separate collection tubes at different time points (12, 24, and 48 h) after injection. The urine samples were then analyzed by a fluorescence spectrometer. For *in vivo* biodistribution studies, the tumor-bearing mouse model was first established: an MCF-7 cell suspension (0.2 mL, 1×10^7 cells mL^{-1}/mouse) was injected subcutaneously into the mice. When the tumor grew to about 100 cm^3, the nanoparticles (20 mg/kg) were administered by tail vein injection. The mice were killed after injection for 24 and 48 h, and heart, liver, spleen, lung, kidneys, and tumor were collected. The tissues were weighed, digested, and then analyzed for silicon content using ICP-OES.

Drug Loading and Release Behaviors. To load DOX into MSNs and MSNs/HAP, 100 mg of nanoparticles was dispersed into 1.7 mL of DOX solution (3 mg/mL), and the mixed solutions were kept at 4 °C for 24 h to reach maximum DOX loading. Then the dispersion was centrifuged to separate the drug-loaded nanoparticles, which were washed with distilled water three times. Drug loading efficiency was calculated according to the following equation:

$$\text{Drug loading efficiency } (\%) = 100 \times W_{\text{DOX}}/W_{\text{NPs-DOX}}$$

where W_{DOX} is the weight of DOX loaded into the nanoparticles and $W_{\text{NPs-DOX}}$ is the weight of MSNs-DOX and MSNs/HAP-DOX.

To measure the drug release behavior, drug-loaded NPs were redispersed in 3 mL of PBS (pH = 7.4) or acetic acid buffer solution (pH = 5.0) and transferred to a dialysis bag (molecular weight cut-off 7000 Da). Then the bag was subsequently placed in a 50 mL centrifuge tube containing 27 mL of corresponding buffer solution. A 15 mL amount of solution was sampled from the tube every half an hour during the first 3 h and then sampled every day. The volume of the release system in the tube was kept constant by adding an equal volume of fresh buffer solution. The released DOX dose of the samples was determined by a UV−vis/near-infrared spectrophotometer (Lambda 950, PerkinElmer Instruments Co. Ltd., USA) with the detection wavelength of 485 nm. All release samples were averaged with three measurements.[46]

Cytotoxicity Assay. MTT was used to investigate the cytotoxicity of the nanoparticles on human breast cancer cells (MCF-7).[47] Cells were maintained in DMEM complete medium (GIBCO) supplemented with 10% (v/v) FBS, cultured in a humidified atmosphere containing 5% CO_2 at 37 °C. For the MTT assay, cells were seeded into 96-well plates with a density of 5000 per well and incubated for 24 h to allow cell attachment. Then free DOX, DOX@MSNs, and DOX@MSNs/HAP were added respectively at a certain amount of DOX concentration ranging from 0.08 to 20 μg/mL. After 48 h, the culture media were replaced by fresh media containing MTT (0.5 mg/mL), and the cells were incubated for an additional 4 h. Upon removing MTT solution, the purple formazan crystals were dissolved with 100 μL of dimethyl sulfoxide (DMSO) and the absorbance was recorded at 570 nm with a microplate reader (TECAN Znfinite M200, Austria). Untreated cells in the medium were used as a control. Corresponding groups without cells were used as blanks. All experiments were carried out with four replicates.

Intracellular Drug Release Assay. MCF-7 cells were incubated with free DOX, DOX@MSNs, and DOX@MSNs/HAP for 2 h in Petri dishes, then washed with PBS three times, and subsequently labeled with the fluoroprobe Lysoracker Green in the culture medium at 37 °C for 30 min. After labeling, cells were washed with PBS buffer to remove the residual DOX or nanoparticles. The intracellular localizations of free DOX and released DOX from drug-loaded nanocarriers were directly visualized *via* a confocal laser scanning microscope (Carl Zeiss, Germany). Lysotracker Green was excited at 488 nm, and its emission was recorded at 535 nm. DOX was excited at 488 nm, and its emission was recorded at 560−600 nm. All experiments were carried out under light-sealed conditions to avoid photobleaching.[46]

Hemolysis Assay. Blood compatibility was evaluated with a hemolysis assay. Fresh rat blood was extracted from the hepatic vein and stabilized with heparin. A 2 mL sample of whole blood was added to 4 mL of Dulbecco's phosphate-buffered saline (D-PBS) and then centrifuged at 10016*g* for 5 min to isolate red blood cells. The RBCs were further washed five times with 10 mL of D-PBS and finally diluted to 20 mL of D-PBS. A 0.2 mL amount of diluted RBC suspension was exposed to 0.8 mL of the nanoparticle suspension in D-PBS at a concentrations of 2.5, 12.5, 62.5, 125, 250, or 500 μg/mL to make the final nanoparticle concentration 2, 10, 50, 100, 200, or 400 μg/mL (test group), distilled water (positive group), and D-PBS (negative group). Every group was represented for four tubes. After incubation at room temperature for 4 h and centrifugation for 5 min, 100 μL of the supernatant of all samples was transferred to a 96-well plate and the absorbance was measured by a microplate reader at 577 nm with 655 nm as a reference. The hemolytic degree was expressed by the hemolytic ratio using the following formula:

$$\text{Hemolysis ratio} = (\text{OD}_{\text{test}} - \text{OD}_{\text{negative control}})/(\text{OD}_{\text{positive control}} - \text{OD}_{\text{negative control}}) \times 100\%$$

Evaluation of *in Vivo* Antitumor Activity. The tumor-bearing mouse model was established as above. The tumor-bearing mice were randomly divided into four groups: (a) saline; (b) free DOX; (c) DOX@MSNs; (d) DOX@MSNs/HAP. Drugs were administered by intravenous injection at 3-day intervals, and the doses of DOX@MSNs and DOX@MSNs/HAP were calculated based on DOX equivalence of 2.5 mg/kg. The tumor size (L, length; W, width) and body weight were measured twice a week. Tumor volume (TV) was calculated as follows: $TV = {}^{1}/_{2}LW^2$. Relative weight (RW) was calculated according to the formula $RW = W_i/W_o$, where W_o is the mean weight at the beginning of treatment and W_i is the mean weight at any subsequent time point.[48]

Biochemical Assay of Serum. At the end of the period, all mice were anaesthetized with ether and then sacrificed. Blood samples were obtained from ophthalmic veins and collected into a clotted vial. After being centrifuged, the serum was used for biochemical analysis. The study was conducted at the Laboratory Animals Center of Chinese PLA General Hospital (301 Hospital, Beijing), under a protocol approved by the ethics committee of the hospital. TBIL, ALT, and AST in serum were measured to evaluate liver function. UA, Cr, BUN, and T-prot in serum were measured to evaluate nephrotoxicity by an automatic biochemical analyzer (7600-110, Hitachi, Tokyo).

Histological Analysis. After blood collection, the heart, liver, and kidneys were removed. A part of the tissues were fixed in 10% formalin solution for histopathological studies. Fixed organs were embedded in paraffin blocks, cut into 5 μm thick slices, and then placed on glass slides. Haematoxylin and eosin-stained histological sections were observed with light microscopy (BX53, Olympus, Japan).

Conflict of Interest: The authors declare no competing financial interest.

Acknowledgment. This work was supported by Natural Science Foundation projects (31470961, 21001038, 21271059, 21301046, 51302062, 30970784, 81171455), National Key Basic Research Program of China (2009CB930200), Research Fund for the Doctoral Program of Higher Education of China (20111301110004, 20131301120004), Key Basic Research Special Foundation of Science Technology Ministry of Hebei Province (14961302D), Hebei Province "Hundred Talents Program" (BR2-202), Hebei Province "Three Three Three Talents Program" (A201401002), China Postdoctoral Science Foundation Funded Project (2013M530119, 2014T70226), Key Program of Hebei University Scientific Research Project (ZD2015031), Natural Science Foundation of Hebei Province (B2015201097), Hebei Provincial Department of Education Project (205020515519), Training Program for Innovative Research Team and Leading Talent in Hebei Province University (LJRC024), CAS "Hundred Talents Program" (07165111ZX), 2G12RR003048 from the RCMI program, the Research Fund of State Key Laboratory of Rare Earth Resource Utilization (RERU2015025), and SRF for ROCS, SEM.

Supporting Information Available: The Supporting Information is available free of charge on the ACS Publications website at DOI: 10.1021/nn507485j.

Additional figures as described in the text (PDF)

REFERENCES AND NOTES

1. Timko, B. P.; Whitehead, K.; Gao, W. W.; Kohane, D. S.; Farokhzad, O.; Anderson, D.; Langer, D. Advances in Drug Delivery. *Annu. Rev. Mater. Res.* **2011**, *41*, 1–20.
2. Brigger, I.; Dubernet, C.; Couvreur, P. Nanoparticles in Cancer Therapy and Diagnosis. *Adv. Drug Delivery Rev.* **2002**, *54*, 631–651.
3. Haley, B.; Frenkel, E. Nanoparticles for Drug Delivery in Cancer Treatment. *Urol. Oncol.-Semin.Origi.* **2008**, *26*, 57–64.
4. Lasic, D. D. Novel Applications of Liposomes. *Trends Biotechnol.* **1998**, *16*, 307–321.
5. Liechty, W. B.; Peppas, N. A. Expert Opinion: Responsive Polymer Nanoparticles in Cancer Therapy. *Eur. J. Pharm. Biopharm.* **2012**, *80*, 241–246.
6. Huo, S. D.; Ma, H. L.; Huang, K. Y.; Liu, J.; Wei, T.; Jin, S. B.; Zhang, J. C.; He, S. T.; Liang, X. J. Superior Penetration and Retention Behavior of 50 nm Gold Nanoparticles in Tumors. *Cancer Res.* **2013**, *73*, 319–330.
7. Parveen, S.; Misra, R.; Sahoo, S. K. Nanoparticles: A Boon to Drug Delivery, Therapeutics, Diagnostics and Imaging. *Nanomedicine* **2012**, *8*, 147–166.
8. De Jong, W. H.; Borm, P. J. A. Drug Delivery and Nanoparticles: Applications and Hazards. *Int. J. Nanomed.* **2008**, *3*, 133–149.
9. Dasgupta, S.; Banerjee, S. S.; Bandyopadhyay, A.; Bose, S. Zn- and Mg-Doped Hydroxyapatite Nanoparticles for Controlled Release of Protein. *Langmuir* **2010**, *26*, 4958–4964.
10. Meng, H. A.; Liong, M.; Xia, T. A.; Li, Z. X.; Ji, Z. X.; Zink, J. I.; Nel, A. E. Engineered Design of Mesoporous Silica

Nanoparticles to Deliver Doxorubicin and P-Glycoprotein siRNA to Overcome Drug Resistance in a Cancer Cell Line. *ACS Nano* **2010**, *4*, 4539–4550.

11. Xia, T. A.; Kovochich, M.; Liong, M.; Meng, H.; Kabehie, S.; George, S.; Zink, J. I.; Nel, A. E. Polyethyleneimine Coating Enhances the Cellular Uptake of Mesoporous Silica Nanoparticles and Allows Safe Delivery of siRNA and DNA Constructs. *ACS Nano* **2009**, *3*, 3273–3286.
12. Chen, J. F.; Ding, H. M.; Wang, J. X.; Shao, L. Preparation and Characterization of Porous Hollow Silica Nanoparticles for Drug Delivery Application. *Biomaterials* **2004**, *25*, 723–727.
13. Li, Z. Z.; Xu, S. A.; Wen, L. X.; Liu, F.; Liu, A. Q.; Wang, Q.; Sun, H. Y.; Yu, W.; Chen, J. F. Controlled Release of Avermectin from Porous Hollow Silica Nanoparticles: Influence of Shell Thickness on Loading Efficiency, UV-Shielding Property and Release. *J. Controlled Release* **2006**, *111*, 81–88.
14. Zhang, S. L.; Chu, Z. Q.; Yin, C.; Zhang, C.; Lin, G.; Li, Q. Controllable Drug Release and Simultaneously Carrier Decomposition of SiO_2-Drug Composite Nanoparticles. *J. Am. Chem. Soc.* **2013**, *135*, 5709–5716.
15. Park, J. H.; Gu, L.; von Maltzahn, G.; Ruoslahti, E.; Bhatia, S. N.; Sailor, M. J. Sailor, M. J. Biodegradable Luminescent Porous Silicon Nanoparticles for *In Vivo* Applications. *Nat. Mater.* **2009**, *8*, 331–336.
16. Pohaku Mitchell, K. K.; Liberman, A.; Kummel, A. C.; Trogler, W. C. Iron(III)-Doped, Silica Nanoshells: a Biodegradable Form of Silica. *J. Am. Chem. Soc.* **2012**, *134*, 13997–4003.
17. Alexis, F.; Pridgen, E.; Molnar, L. K.; Farokhzad, O. C. Factors Affecting the Clearance and Biodistribution of Polymeric Nanoparticles. *Mol. Pharmaceutics* **2008**, *5*, 505–515.
18. He, Q.; Shi, J. Mesoporous Silica Nanoparticles Based Nano Drug Delivery Systems: Synthesis, Drug Controlled Release and Delivery, Pharmacokinetics and Biocompatibility. *J. Mater. Chem.* **2011**, *21*, 5845–5855.
19. Huang, X.; Li, L.; Liu, T.; Hao, N.; Liu, H.; Chen, D.; Tang, F. The Shape Effect of Mesoporous Silica Nanoparticles on Biodistribution, Clearance, and Biocompatibility *In Vivo*. *ACS Nano* **2011**, *5*, 5390–5399.
20. Lee, C. H.; Cheng, S. H.; Wang, Y. J.; Chen, Y. C.; Chen, N. T.; Souris, J.; Chen, C. T.; Mou, C. Y.; Yang, C. S.; Lo, L. W. Near-Infrared Mesoporous Silica Nanoparticles for Optical Imaging: Characterization and *In Vivo* Biodistribution. *Adv. Funct. Mater.* **2009**, *19*, 215–222.
21. Lu, J.; Liong, M.; Li, Z.; Zink, J. I.; Tamanoi, F. Biocompatibility, Biodistribution, and Drug-Delivery Efficiency of Mesoporous Silica Nanoparticles for Cancer Therapy in Animals. *Small* **2010**, *6*, 1794–1805.
22. Dai, C.; Yuan, Y.; Liu, C.; Wei, J.; Hong, H.; Li, X.; Pan, X. Degradable, Antibacterial Silver Exchanged Mesoporous Silica Spheres for Hemorrhage Control. *Biomaterials* **2009**, *30*, 5364–5375.
23. Nabeshi, H.; Yoshikawa, T.; Matsuyama, K.; Nakazato, Y.; Matsuo, K.; Arimori, A.; Isobe, M.; Tochigi, S.; Kondoh, S.; Hirai, T. Systemic Distribution, Nuclear Entry and Cytotoxicity of Amorphous Nanosilica Following Topical Application. *Biomaterials* **2011**, *32*, 2713–2724.
24. Nabeshi, H.; Yoshikawa, T.; Matsuyama, K.; Nakazato, Y.; Tochigi, S.; Kondoh, S.; Hirai, T.; Akase, T.; Nagano, K.; Abe, Y. Amorphous Nanosilica Induce Endocytosis-dependent ROS Generation and DNA Damage in Human Keratinocytes. *Part. Fibre Toxicol.* **2011**, *8*, 1.
25. Yamashita, K.; Yoshioka, Y.; Higashisaka, K.; Mimura, K.; Morishita, Y.; Nozaki, M.; Yoshida, T.; Ogura, T.; Nabeshi, H.; Nagano, K. Silica and Titanium Dioxide Nanoparticles Cause Pregnancy Complications in Mice. *Nat. Nanotechnol.* **2011**, *6*, 321–328.
26. Pohaku Mitchell, K. K.; Liberman, A.; Kummel, A. C.; Trogler, W. C. Iron (III)-doped, Silica Nanoshells: A Biodegradable Form of Silica. *J. Am. Chem. Soc.* **2012**, *134*, 13997–14003.
27. Li, X.; Zhang, L.; Dong, X.; Liang, J.; Shi, J. Preparation of Mesoporous Calcium Doped Silica Spheres with Narrow Size Dispersion and Their Drug Loading and Degradation Behavior. *Microporous Mesoporous Mater.* **2007**, *102*, 151–158.
28. Schlossbauer, A.; Warncke, S.; Gramlich, P. M. E.; Kecht, J.; Manetto, A.; Carell, T.; Bein, T. A Programmable DNA-Based Molecular Valve for Colloidal Mesoporous Silica. *Angew. Chem., Int. Ed.* **2010**, *49*, 4734–4737.
29. Rim, H. P.; Min, K. H.; Lee, H. J.; Jeong, S. Y.; Lee, S. C. pH-Tunable Calcium Phosphate Covered Mesoporous Silica Nanocontainers for Intracellular Controlled Release of Guest Drugs. *Angew. Chem., Int. Ed.* **2011**, *50*, 8853–8857.
30. Liu, J. A.; Bu, W. B.; Pan, L. M.; Shi, J. L. NIR-Triggered Anticancer Drug Delivery by Upconverting Nanoparticles with Integrated Azobenzene-Modified Mesoporous Silica. *Angew. Chem., Int. Ed.* **2013**, *52*, 4375–4379.
31. Bernardos, A.; Aznar, E.; Marcos, M. D.; Martinez-Manez, R.; Sancenon, F.; Soto, J.; Barat, J. M.; Amoros, P. Enzyme-Responsive Controlled Release Using Mesoporous Silica Supports Capped with Lactose. *Angew. Chem., Int. Ed.* **2009**, *48*, 5884–5887.
32. Aznar, E.; Marcos, M. D.; Martinez-Manez, R.; Sancenon, F.; Soto, J.; Amoros, P.; Guillem, C. pH- and Photo-Switched Release of Guest Molecules from Mesoporous Silica Supports. *J. Am. Chem. Soc.* **2009**, *131*, 6833–6843.
33. Zhang, J.; Yuan, Z. F.; Wang, Y.; Chen, W. H.; Luo, G. F.; Cheng, S. X.; Zhuo, R. X.; Zhang, X. Z. Multifunctional Envelope-Type Mesoporous Silica Nanoparticles for Tumor-Triggered Targeting Drug Delivery. *J. Am. Chem. Soc.* **2013**, *135*, 5068–5073.
34. Wang, Y.; Wang, K.; Zhao, J.; Liu, X.; Bu, J.; Yan, X.; Huang, R. Multifunctional Mesoporous Silica-Coated Graphene Nanosheet Used for Chemo-Photothermal Synergistic Targeted Therapy of Glioma. *J. Am. Chem. Soc.* **2013**, *135*, 4799–4804.
35. Zhang, C.; Yang, J.; Quan, Z.; Yang, P.; Li, C.; Hou, Z.; Lin, J. Hydroxyapatite Nano- and Microcrystals with Multiform Morphologies: Controllable Synthesis and Luminescence Properties. *Cryst. Growth Des.* **2009**, *9*, 2725–2733.
36. Zhang, C.; Li, C.; Huang, S.; Hou, Z.; Cheng, Z.; Yang, P.; Peng, C.; Lin, J. Self-Activated Luminescent and Mesoporous Strontium Hydroxyapatite Nanorods for Drug Delivery. *Biomaterials* **2010**, *31*, 3374–3383.
37. Ahsan, R.; Mortuza, M. G. Infrared Spectra of xCaO(1-x-z)-SiO(2)zP(2)O(5) Glasses. *J. Non-Cryst. Solids* **2005**, *351*, 2333–2340.
38. Barbe, C.; Bartlett, J.; Kong, L.; Finnie, K.; Lin, H. Q.; Larkin, M.; Calleja, S.; Bush, A.; Calleja, G. Silica Particles: A Novel Drug-Delivery System. *Adv. Mater.* **2004**, *16*, 1959–1966.
39. Tzur-Balter, A.; Shatsberg, Z.; Becherman, M.; Segal, E.; Artzi, N. Mechanism of Erosion of Nanostructured Porous Silicon Drug Carriers in Neoplastic Tissues. *Nat. Commun.* **2015**, *6*, 6208–6216.
40. Tasciotti, E.; Liu, X.; Bhavane, R.; Plant, K.; Leonard, A. D.; Price, B. K.; Cheng, M. M.; Decuzzi, P.; Tour, J. M.; et al. Mesoporous Silicon Particles as a Multistage Delivery System for Imaging and Therapeutic Applications. *Nat. Nanotechnol.* **2008**, *3*, 151–157.
41. Gu, L.; Hall, D. J.; Qin, Z.; Anglin, E.; Joo, J.; Mooney, D. J.; Howell, S. B.; Sailor, M. J. *In Vivo* Time-Gated Fluorescence Imaging with Biodegradable Luminescent Porous Silicon Nanoparticles. *Nat. Commun.* **2013**, *4*, 2326.
42. Yu, T.; Malugin, A.; Ghandehari, H. Impact of Silica Nanoparticle Design on Cellular Toxicity and Hemolytic Activity. *ACS Nano* **2011**, *5*, 5717–5728.
43. Slowing, I. I.; Wu, C. W.; Vivero-Escoto, J. L.; Lin, V. S. Y. Mesoporous Silica Nanoparticles for Reducing Hemolytic Activity towards Mammalian Red Blood Cells. *Small* **2009**, *5*, 57–62.
44. Lin, Y. S.; Haynes, C. L. Impacts of Mesoporous Silica Nanoparticle Size, Pore Ordering, and Pore Integrity on Hemolytic Activity. *J. Am. Chem. Soc.* **2010**, *132*, 4834–4842.
45. Wang, J.; Chen, C.; Li, B.; Yu, H.; Zhao, Y.; Sun, J.; Li, Y.; Xing, G.; Yuan, H.; Tang, J.; et al. Antioxidative Function and Biodistribution of $[Gd@C_{82}(OH)_{22}]_n$ Nanoparticles in Tumor-Bearing Mice. *Biochem. Pharmacol.* **2006**, *71*, 872–881.
46. Hu, X. X.; Hao, X. H.; Wu, Y.; Zhang, J. C.; Zhang, X. N.; Wang, P. C.; Zou, G. Z.; Liang, X. J. Multifunctional Hybrid Silica

Nanoparticles for Controlled Doxorubicin Loading and Release with Thermal and pH Dual Response. *J. Mater. Chem. B* **2013**, *1*, 1109–1118.

47. Mosmann, T. Rapid Colorimetric Assay for Cellular Growth and Survival: Application to Proliferation and Cytotoxicity Assays. *J. Immunol. Methods* **1983**, *65*, 55–63.
48. Meng, J.; Xing, J.; Wang, Y.; Lu, J.; Zhao, Y.; Gao, X.; Wang, P. C.; Jia, L.; Liang, X. Epigenetic Modulation of Human Breast Cancer by Metallofullerenol Nanoparticles: *In Vivo* Treatment and *In Vitro* Analysis. *Nanoscale* **2011**, *3*, 4713–4719.